JOURNAL OF BIOMEDICAL OPTICS 1(3), 342–355 (JULY 1996)

OPTICAL PROPERTIES OF NORMAL AND DISEASED BREAST TISSUES: PROGNOSIS FOR OPTICAL MAMMOGRAPHY

Tamara L. Troy,[†] David L. Page,[‡] and Eva M. Sevick-Muraca[†]
[†]Purdue University, School of Chemical Engineering, West Lafayette, Indiana 47907; [‡]Vanderbilt University, Vanderbilt School of Medicine, Nashville, Tennessee 37235

(Paper JBO-073 received Feb. 7, 1996; revised manuscript received Apr. 11, 1996; accepted for publication Apr. 15, 1996)

ABSTRACT

The use of near-infrared (NIR) measurements of photon migration has been recently demonstrated for the detection of breast cancer in Europe. Yet the clinical success of this potential screening tool depends upon consistent detection of the disease at earlier stages than is currently possible with conventional x-ray mammography. In this paper, we present the optical property measurements of 115 histologically classified breast tissue specimens in order to determine whether consistent and significant optical contrast exists for detection of the disease. Our *in vitro* optical properties measured with a double integrating sphere technique show consistent changes (yet statistically insignificant) in effective scattering coefficients, μ_s', with tissue classification of infiltrating carcinoma (n=48), ductal carcinoma *in situ* (n=5), mucinous carcinoma (n=3), normal fatty (n=23), and normal fibrous tissues (n=35). However, there is little change in the *in vitro* tissue absorption coefficient, μ_a, measured at 749, 789, and 836 nm. For normal and diseased tissue specimens extracted from the *same patient*, we found differences in optical properties, indicating optical contrast. Using a finite-element prediction of light propagation, we evaluated this optical contrast for photon migration detection of ductal carcinoma *in situ* tissues using these optical properties measured *in vitro*.

Keywords optical mamography; photon migration imaging; tissue scattering; tissue absorption; breast cancer screening.

1 INTRODUCTION

One out of every eight women in the U.S. will encounter breast cancer in her lifetime.[1] While x-ray mammography is generally an effective screening tool against the disease, studies have shown that mortality rates in women less than 40–50 years of age are not positively influenced by this screening method. In this age group, x-ray mammography has an unacceptable 50% false negative rate.[2] Consequently, numerous research groups have embarked upon nonionizing, near-infrared (NIR) approaches for detecting and imaging diseased breast tissues. The proposed techniques range from CW (continuous wave) or time-independent measurements of scattered light[3] to snake-light measurements of unscattered light[4,5] and photon migration or time-dependent measurements of multiply scattered light.[6–8] In each of these techniques, light that has been transmitted across several centimeters of tissue is detected.

Perhaps the most promising technique lies with photon migration measurements. Photon migration imaging consists of measuring the time-dependent characteristics of light propagation and then reconstructing an image of normal and diseased tissues based upon their optical properties. Similar to ultrasound and impedance tomography, the reconstructions are based upon an iterative approach in order to converge upon a ''map'' of tissue optical properties which gives the minimum error between the measured photon migration characteristics,[6,9,10] and that predicted by the optical diffusion equation.[11] The endogenous optical contrast for detection of diseased tissues can be provided by (1) the local tissue absorption coefficient, μ_a, which arises primarily due to hemoglobin and increased vascular volumes associated with tumor angiogenesis, and (2) the isotropic tissue scattering coefficient, μ_s', which in the NIR regime arises primarily due to mitochondria[12,13] and predominates over absorption. Numerous investigators report reconstructed images based upon differences in absorption and scattering. O'Leary and co-workers[14] report success in reconstructing images of a 1.0 to 2.0-cm diameter heterogeneity embedded in a 6×6 cm tissue-mimicking scattering medium from experimental photon migration measurements made in the frequency domain (Table 1). Pogue et al.[9] have dem-

Address all correspondence to Eva M. Sevick-Muraca. E-mail: sevick@ecn.purdue.edu

1083-3668/96/$6.00 © 1996 SPIE

Table 1 Summary of simulated and experimental optical properties used for image reconstruction found in literature.

	Surroundings			Heterogeneity		
Reference	Size	μ_a (cm^{-1})	μ_s' (cm^{-1})	Size (diameter)	μ_a (cm^{-1})	μ_s' (cm^{-1})
O'Leary[14]	6×6 cm square	0.023	6.0	1.2	perfect absorber	-
	6×6 cm square	0.023	6.0	1.2	0.023	15
	6×6 cm square	0.1	6.0	1.0 (2 objects)	0.4	6.0
	6×6 cm square	1.0	6.0	1.0 (2 objects)	4.0	6.0
Pogue[9]	8.6 cm diameter cylinder	0.047	4.7	2.5 cylinder	0.075	4.7
	8.6 cm diameter	0.047	4.7	2.5 cylinder	0.047	9.4

	Size	Contrast	Size	Contrast
Barbour[10]	41×41×10 mfp	τ=0.01*	1 mfp^3	τ=0.05*
	~4.1×4.1×0.1 cm for tissue		~1 mm^3 for tissue	$\mu_a = 5\,\mu_a^{surr}$ $\mu_s' = \mu_s'^{surr}$

*$\tau = \left(\frac{\mu_a}{\mu_s + \mu_a}\right)$.

onstrated reconstructions from experimental frequency domain measurements for a 8.6 cm diameter homogeneous medium with a 2.5 cm diameter heterogeneity (Table 1). Their results show that image reconstructions can be severely degraded by boundaries that are unaccounted for. Jiang and Paulsen show reconstruction of 4 mm diameter heterogeneities in an 8.6-cm diameter tissue phantom.[15] Barbour and co-workers[10] show simulations that point to the detection of heterogeneities as small as 1 mfp (~1 mm^3 for tissues) (Table 1). Instead of using reconstructed images, Sevick et al.[16] demonstrated that multipixel measurements of frequency-domain photon migration can be used to construct a phase-shift and amplitude modulation map in order to detect optical heterogeneities directly. Recently, Franceschini and co-workers[17] demonstrated that *in vivo* single-pixel measurements of phase-shift and amplitude modulation may also be used to directly construct an optical mammogram. Their results show that photon migration can effectively detect carcinomas that have been previously identified by x-ray mammography. Thus, the feasibility of photon migration imaging for detecting breast cancer has already been demonstrated. The capabilities improving detectability of the disease beyond that currently possible with conventional x-ray mammography may depend upon (1) the successful implementation of developing image reconstructions and (2) the degree of contrast, $\Delta\mu_a$ and $\Delta\mu_s'$ or the differences in absorption and scattering properties that must exist between normal and diseased tissue for effective detection.

In this article, we present *in vitro* measurements of optical properties of 115 normal and diseased breast tissues characterized by histology in order to assess the optical contrast, or $\Delta\mu_a$ and $\Delta\mu_s'$. In addition, we provide *in vitro* measurements of normal and diseased tissues obtained from five patients in order to assess whether the presence of disease will affect measurement of photon migration and provide detection, whether inversion algorithms or direct imaging techniques are employed. Finally, using the optical properties measured in these studies, we demonstrate the impact of endogenous contrast using finite-element predictions of changes in photon migration due to a tumor embedded in an otherwise homogeneous tissue.

2 EXPERIMENTAL MEASUREMENT OF TISSUE OPTICAL PROPERTIES

Tissue optical property measurements are fraught with difficulties owing to (1) the necessity of ex-

tracting tissues, thereby enabling the drainage of hemoglobin, (2) the maintenance of tissue viability under measurement conditions, and (3) the accuracy of measurement techniques. Nonetheless, the best possible method of measuring normal and diseased optical properties is a noninvasive measurement. For diseased tissues, this would require an accurate ''map'' or image of *in vivo* tissue optical properties. As described earlier, this has yet to be demonstrated using reconstructed images from CW or photon migration measurements. Since we attempt to assess or estimate the contrast required for such measurements and reconstructions, we conduct our optical property measurements of whole normal and diseased breast tissues using *in vitro* techniques, keeping in mind the issues of blood drainage, maintenance of tissue viability, and accuracy of measuring technique.

2.1 TISSUE SPECIMENS

Measurements were conducted on 115 tissue samples collected from 88 patients. The tissue samples were obtained from the Pathology Department at the Vanderbilt University Medical School with prior patient consent. Of the specimens collected, two were freshly obtained from the surgical suite, placed upon ice, and transported to the Engineering School for optical property measurements. Since freshly excised tissue samples were generally not available and since we found that optical properties were not influenced by freezing and subsequent thawing (see Sec. 2.4), the remainder of our samples were frozen specimens. All specimens were procured from punch biopsy from tissues obtained from lumpectomies, mastectomies, or breast reduction surgeries. The human subject protocol guidelines of Vanderbilt and Purdue universities were strictly followed.

For optical property measurements, fresh or thawed tissue samples were carefully cut into approximately 1-mm-thick slices using a scalpel and taking care to avoid tissue compression. Previously frozen samples were thawed at room temperature. The tissue slices were wetted with saline and placed between two microscope slides, which were then sealed with silicon gel to prevent dehydration. The addition of saline also prevented tissue–glass mismatch of refractive index.[18] Caliper measurements were then made to provide an accurate measurement of the tissue sample thickness. For heterogeneous samples, more than one tissue section was optically examined.

Following optical property measurements, tissue samples were placed in formalin for storage and transport back to the Vanderbilt pathology laboratories. There the samples were embedded in paraffin, sectioned, and stained with hematoxylin and eosin, and mounted on microscope slides for histopathological examination. The pathology of each sample was classified into one of five categories: infiltrating carcinoma, ductal carcinoma *in situ*, mucinous carcinoma, normal fatty, or normal fibrous tissues. In the case of disease, observations of high-, intermediate-, and low-grade carcinomas were reported along with the percentage of diseased tissue content in the specimen as determined by the pathologist.

2.2 DOUBLE INTEGRATING SPHERE MEASUREMENTS OF TISSUE OPTICAL PROPERTIES

Figure 1 illustrates the double integrating sphere apparatus used to measure the diffuse reflectance and transmittance in order to determine tissue optical properties of each specimen. For a complete description of integrating sphere technology, the reader is directed to other excellent treatises on the subject.[19] The tissue specimen was placed between two 15.2 cm diameter integrating spheres (70451, Oriel, Stratford, Connecticut) with internal baffles positioned to prevent measurement of directly reflected or transmitted light. The tissue sample was maintained at 37° Celsius by forced convection using a temperature controller and temperature probe (Fisher Scientific, Atlanta, Georgia).

Diffuse transmitted and reflected light was measured with sample illumination at 749, 789, and 830 nm provided by 5, 30, and 40 mW collimated laser diodes (06DLS103, 06DLS403, 06DLS503, Melles Griot, Carlsbad, California). The beam was elliptical with 1.3×4.0-mm axes, and the sample port was reduced to 12 mm because of the limited size of tissue specimens available. Photodetector (71822, Oriel, Stratford, Connecticut) signals were amplified (70710, Oriel, Stratford, Connecticut) to record diffuse reflectance and transmittance from the first and second spheres respectively. Signals were acquired by a standard computer A/D acquisition, and detector calibrations were performed with reflectance standards (70497, Oriel, Stratford, Connecticut).[18] From diffuse reflectance and transmittance measurements, values of scattering and absorption were obtained using the inverse adding doubling program provided by Professor Scott Prahl at the Laser Research Center at St. Vincent Hospital, Portland, Oregon. These computations assumed an anisotropy parameter, g, equal to 0.9.[20] On each specimen, the incident beam was focused onto three different locations. The results of tissue absorption and scattering are reported as the mean $\pm$ the standard deviation of the values obtained from the three measurements made on the same sample.

2.3 VALIDATION OF OPTICAL PROPERTY MEASUREMENTS

In order to validate the double integrating sphere and inverse adding doubling procedures used, we determined the scattering and absorption coefficients of monodisperse polystyrene microsphere

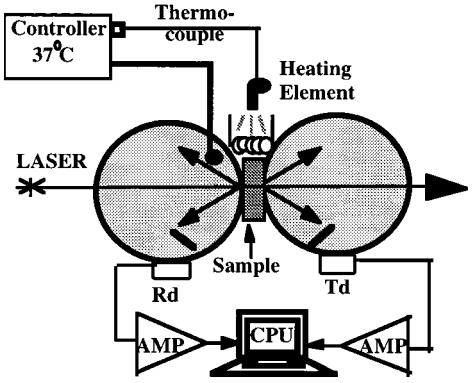

Fig. 1 Schematic of the double integrating sphere apparatus.

suspensions with and without the addition of a broadband absorbing dye. A comparison of results with theoretical predictions provided confidence of our measurement of tissue optical properties.

2.3.1 Scattering Coefficients of Monodisperse Polystyrene

In a 100×100×1-mm glass sample chamber constructed from microscope slide glass (Erie Scientific, Portsmouth, New Hampshire), monodisperse polystyrene suspensions (Polysciences, Inc., Warrington, Pennsylvania) of radii 0.101, 0.185, 0.390, 0.475, 0.719, and 1.043 μm and concentrations varying between 0.625 and 2.5% by volume were examined at 633 (05-LLR-811, Melles Griot, Irvine, CA), 749, and 836 nm in the apparatus shown in Figure 1. Values for the anisotropy parameter, g, for each suspension were computed from Mie scattering theory.[21] Together with measurement of diffuse reflectance and transmittance, values of scattering and absorption were obtained from the inverse adding doubling algorithm. A value of 1.60 was assumed for the refractive index of polystyrene.[22] The values of scattering obtained from experimental measurements and the inverse adding doubling algorithm were then assumed to be linearly related to the volume fraction, ϕ, via the expression [where $\mu'_s = \mu_s(1-g)$]:

$$\mu_s = \frac{Q_{\text{scat}}\pi r^2}{\frac{4}{3}\pi r^3}\,\phi. \tag{1}$$

From measurements of scattering μ_s versus volume fraction ϕ for each microsphere radii r we computed the Mie scattering efficiency, Q_{scat}. Figure 2 shows the typical agreement between Q_{scat}/r predicted by Mie scattering theory and that obtained from integrating sphere measurements at 633, 749, and 836 nm. These results validate the measurement of scattering coefficient from the integrating sphere technique.

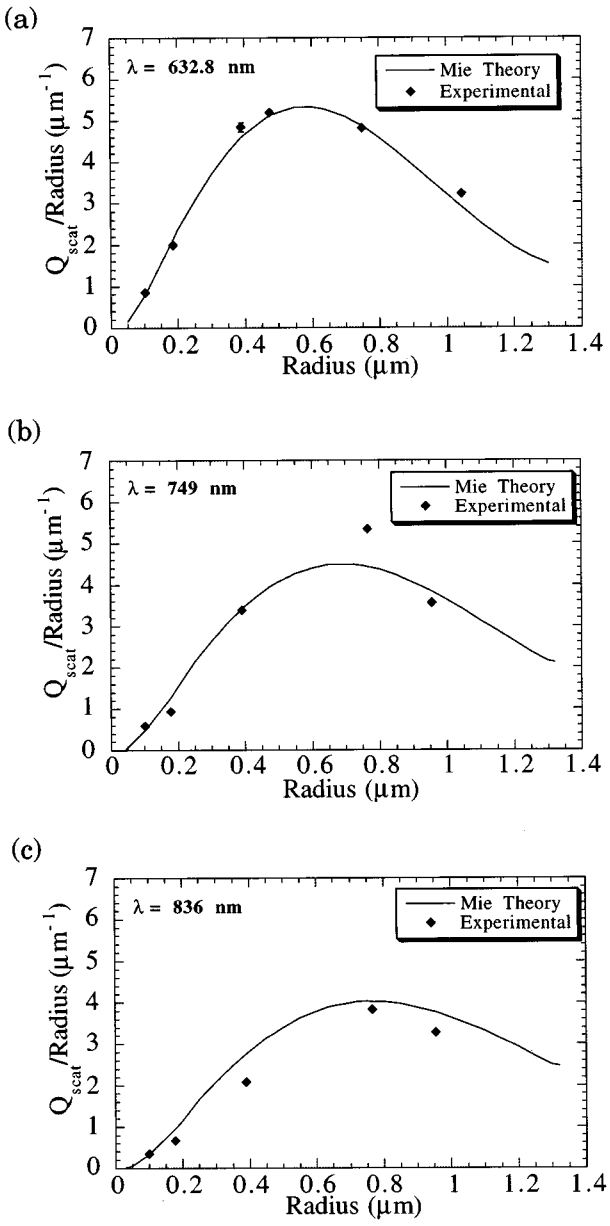

Fig. 2 The efficiency of scatter (Q_{scat}) divided by the particle radius versus the particle radius at wavelengths of (a) 632.8, (b) 749, and (c) 836 nm where the solid line represents that predicted by Mie scattering theory and the symbols are the measured values from the integrating sphere technique.

2.3.2 Absorption Coefficient Measurements of Monodisperse Polystyrene Microspheres

Since light losses may be significant when the ratio of beam diameter to sample port diameter is less than 0.04,[18] we expected the measured absorption properties to be overestimated by double integrating sphere measurements. In order to account for light losses, absorption and scattering coefficients of a monodisperse polystyrene suspension with added absorber were measured and compared against theoretical predictions of scattering coefficients that were computed from Mie theory and ab-

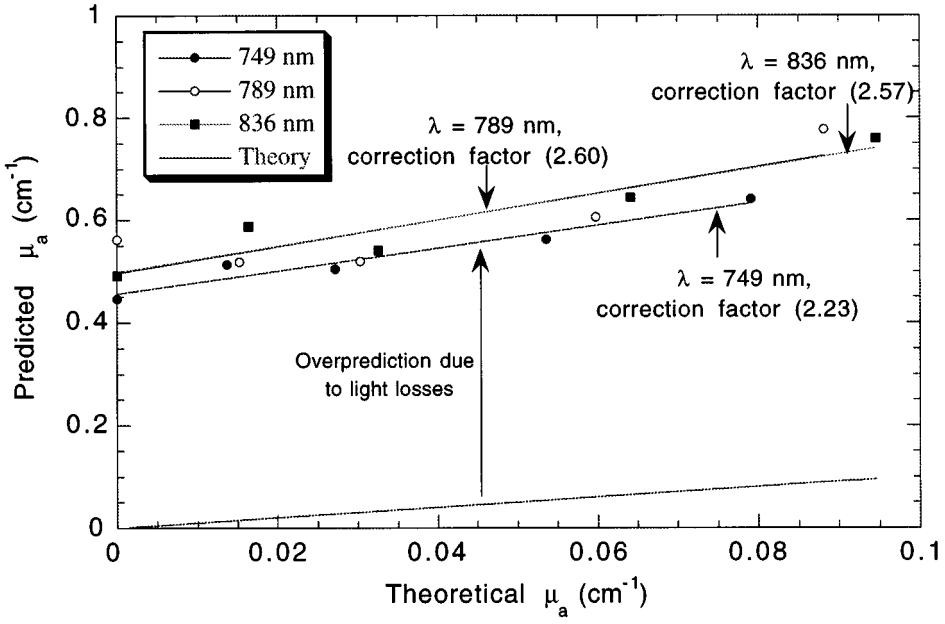

Fig. 3 The predicted absorption coefficient μ_a measured by the integrating spheres and the inverse adding doubling algorithm versus the theoretical μ_a. The slopes are 2.23, 2.60, and 2.57, and intercepts are 0.457, 0.497, and 0.498 for λ=749, 789, and 836 nm respectively.

sorption coefficients that were obtained spectroscopically from nonscattering solutions of a broadband absorber (S109554, Imperial Chemical Industries, Manchester, England). A microsphere 0.53 μm in radius was chosen since its anisotropy parameter most closely corresponded to tissue at the wavelengths studied. Small amounts of dye were introduced so that the final absorption coefficient μ_a was between 0 and 0.1 cm^{-1} in a suspension of microspheres with an isotropic scattering coefficient μ_s' of around 12 cm^{-1}.

From measurements of diffuse reflectance and transmittance, accurate measurements of scattering coefficients were found as the dye concentration increased (data not shown for brevity). However, as shown in Figure 3, light losses due to the small port size caused a consistent overestimation of the absorption coefficient obtained from the double integrating sphere measurement and the inverse-adding doubling algorithm. Since the relationship between the true and the measured absorption coefficient remained consistent within the range of wavelengths studied and within the range of microsphere sizes and concentrations employed, we used the slopes and intercepts of Figure 3 to correct for tissue absorbance measurements. Previous investigators also have employed correction factors (S. L. Jacques, personal communication, Jan. 11, 1995), Monte Carlo corrections,[23] and larger port sizes,[24] to correct for the artifact of light losses. Since tissue extraction causes drainage of blood and the absorption coefficient may be dramatically affected, we used the correction factor as an approach to estimate tissue absorbance. Due to the restrictions of obtaining larger tissue specimens, we were unable to employ a smaller beam-to-port size ratio to minimize light losses.

2.4 VALIDATION OF TISSUE SPECIMEN MEASUREMENT

Since it was anticipated that frozen tissue specimens would have different optical properties than freshly harvested samples, we evaluated the impact of freezing and subsequent thawing at room temperature on the optical properties obtained from the double integrating sphere measurements. Two freshly harvested normal tissue samples were repeatedly frozen in liquid nitrogen and thawed for optical property measurement at 633 nm. On a 99% confidence level, there was no significant difference in the optical properties between previously frozen and thawed tissue specimens. Even though histological evidence shows the morphological changes with freeze/thaw, the mitochondrial compartment, which may be the major cellular constituent responsible for tissue scatter,[12,13] remains intact and presumably provides constant tissue scattering properties (B. Chance, personal communication).

On the other hand, when diffuse reflectance and transmittance measurements are conducted at different temperatures, large differences exist in tissue optical properties. For example, Figure 4 illustrates the temperature dependence of the optical property measurements of the canine prostate. With increasing temperatures, the scattering coefficient increases dramatically, owing to the degradation of cellular components.

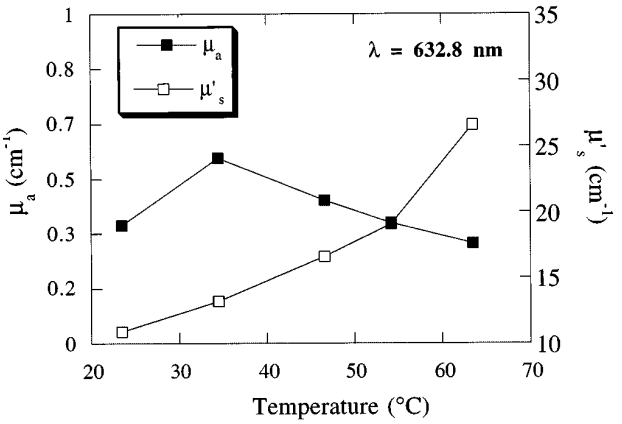

Fig. 4 Absorption coefficient μ_a (open square) and isotropic scattering coefficient μ_s' (closed square) of canine prostate tissue as a function of temperature measured at a wavelength of 632.8 nm.

3 EXPERIMENTAL MEASUREMENTS PREDICTING μ_a AND $\mu_{S'}$ OF POOLED NORMAL AND DISEASED BREAST TISSUES

Table 2 is a comprehensive listing of the scattering and absorption coefficients at each wavelength, as well as the histological classification and comments for each tissue specimen in the current study. Each tissue was classified into one of five groups: infiltrating carcinoma, ductal carcinoma *in situ*, mucinous carcinoma, normal fatty, and normal fibrous tissues. As shown in Table 2, correction of absorbances resulted in some small negative values. In these cases the standard deviation of the measurement was larger than the mean, indicating inaccurate measurement and prediction of μ_a. Since the error in μ_a due to blood loss is unavoidable in this study, we did not attempt to make further corrections as others have done using Monte Carlo techniques.[23,25] Figures 5(a) through 5(c) illustrate the compilation of scattering and absorption coefficients of normal and diseased tissues which include the groupings of fibrous and fatty (open circles) tissues and of infiltrating carcinoma, ductal carcinoma *in situ*, and mucinous disease classifications (closed circles). Since no distinct population of normal versus diseased tissues is apparent in our scatter plots and since there is no statistical difference in optical properties between these two groupings, we evaluated the optical properties of individual classifications (Table 3). In addition, we found no correlation of normal and/or diseased tissues with age and optical properties.

Table 3 lists the optical properties for tissues classified into each of the five categories. While there is no statistical difference between the absorption and scattering properties of normal fatty and normal fibrous tissues, our results show that the scattering coefficient of fatty tissues is lower than that of fibrous tissues. Fatty tissues are identified by the presence of a mature adipose tissue component that is histologically transparent, while fibrous normal tissues exhibit glandular components that have variations in the density of epithelial glands and ducts. Our optical property measurements reflect these morphological differences, which are illustrated in Figure 6(a). Peters et al.[25] have also measured the optical properties of several homogenized breast tissues. They report that the scattering coefficient of homogenized adipose tissues is smaller than that of homogenized glandular and fibrocystic tissues, which is consistent with our results. However, no direct comparisons can be made since their tissue measurements were conducted at room temperature and their specimens were homogenized for tissue uniformity.

Mucinous carcinoma is a comparatively rare disease in which cancer cells secrete extracellular mucin, thereby providing a transparent tissue component in which cancer cells float or reside. An example of a mucinous carcinoma is illustrated in Figure 6(b). Interestingly, Table 3 shows that the scattering coefficient of mucinous carcinoma samples is statistically smaller than infiltrating carcinoma at an 80% confidence level at 749 and 836 nm and at a 90% confidence level at 789 nm. Differences in the scattering coefficient between mucinous carcinoma and ductal carcinoma *in situ* occur at a 90% confidence level for 749 and 789 nm and at 80% for 836 nm. The scattering coefficient of mucinous carcinoma was found to be statistically lower than fibrous tissues at a 95% confidence level for all wavelengths studied. No difference in the scattering coefficient between mucinous carcinoma and fatty tissues was found at 749 nm, but at an 80% confidence level, mucinous carcinoma was found to be statistically lower at 789 and 836 nm.

Infiltrating carcinoma is characterized by increased cellularity and enlarged nuclei, depending upon its grade. As with the ductal carcinoma *in situ*, the degree of increased cellularity and enlarged nuclei characterize the grade: high-grade carcinomas exhibit high cellularity and nuclei content consistent with the aggressiveness of the disease while low-grade carcinomas exhibit inverse features.[26] While ductal carcinoma *in situ* resembles infiltrating carcinoma, it differs in that it is confined to the ducts. Within the ductal carcinoma *in situ* classifications, there are also variations in histological patterns that are indicative of prognosis.[27] Figures 6(c) and 6(d) are micrographs illustrative of the these two diseased states. Our results show that there is no statistical difference at the 99% confidence levels between these two classifications. In addition, there is no significant statistical difference between the scattering coefficients of infiltrating carcinoma and normal fibrous tissues, and between the scattering coefficients of infiltrating carcinoma and normal fatty tissues. There is no statistical difference between the scattering coefficients of ductal carcinoma *in situ* and normal fibrous tissues, and

Table 2 Optical properties and classificationof human breast tissue samples at wavelengths of 749, 789, and 836 nm.

		λ = 749 nm						λ = 789 nm						λ = 836 nm								
Sample	Type	μ_a(cm^{-1})*			μ_s'(cm^{-1})			μ_a(cm^{-1})*			μ_s'(cm^{-1})			μ_a(cm^{-1})*			μ_s'(cm^{-1})			AGE	Grade	Comments
1	Infiltrating Carcinoma	0.0964	±	0.1727	5.0058	±	1.1233	0.0800	±	0.1671	6.4149	±	0.3152	0.0345	±	6.5044	4.5084	±	1.7185	---	inter-high	30-40% of specimen, 10-20% fat and fibrous in specimen
2a	Infiltrating Carcinoma	0.0864	±	0.2020	11.3210	±	2.1571	0.0364	±	0.1757	9.4108	±	2.8519	0.0525	±	2.5678	7.9581	±	0.7085	76	high	small amount of fat on outside edge
2b	Infiltrating Carcinoma	-0.0064	±	0.1831	9.3455	±	1.1410	-0.0296	±	0.1774	7.4258	±	0.5503	0.1362	±	5.4534	10.7560	±	1.4488	76	high	small amount of fat on outside edge
2c	Infiltrating Carcinoma	0.0516	±	0.1486	11.9172	±	1.9529	0.0168	±	0.1685	9.4636	±	0.7704	-0.0041	±	0.5493	9.2228	±	0.1907	76	high	small amount of fat on outside edge
5	Infiltrating Carcinoma	0.3492	±	0.1852	16.5769	±	0.7960	0.2006	±	0.1777	12.7934	±	0.8754	0.2862	±	0.1797	12.0145	±	0.7139	---	intermediate	30% of specimen
6	Infiltrating Carcinoma	0.0621	±	0.1839	9.9649	±	3.0631	0.0471	±	0.1886	7.5970	±	0.4417	0.0849	±	0.1779	7.3122	±	0.5108	60	---	20-30% of specimen
7a	Infiltrating Carcinoma	0.1126	±	0.1614	15.4877	±	3.3726	0.0556	±	0.1739	13.2244	±	1.4949	0.0307	±	0.1810	5.8903	±	0.4115	---	---	50% of specimen, of cancer 70% fibrous, 20% fat
8	Infiltrating Carcinoma	0.1202	±	0.1892	11.4070	±	0.5682	0.1243	±	0.1839	13.2460	±	1.6609	0.0171	±	0.1309	10.0840	±	1.7515	76	high	50% of specimen, 50% dense fibrous tissue
16	Infiltrating Carcinoma	-0.0088	±	0.1918	10.0930	±	2.2810	0.0310	±	0.1853	5.6404	±	1.4014	0.0800	±	0.1852	8.2151	±	1.8415	56	intermediate	80% of specimen, some benign connective tissue and fat
22a	Infiltrating Carcinoma	0.1757	±	0.1914	16.6563	±	2.9426	0.1074	±	0.1834	13.3750	±	1.4137	0.1882	±	0.1601	13.7790	±	1.6703	---	high	95% of specimen, of cancer 30% fibrous tissue
22b	Infiltrating Carcinoma	0.1742	±	0.1667	12.4370	±	3.2730	0.1195	±	0.1568	13.5600	±	2.7347	0.1595	±	0.1695	12.0340	±	3.7701	---	high	80% connective tissue in specimen
23	Infiltrating Carcinoma	0.1819	±	0.1413	10.6070	±	2.1831	0.0755	±	0.1783	8.4340	±	1.5563	0.2040	±	0.1303	11.2750	±	2.7446	77	high	Cancer throughout entire specimen
24	Infiltrating Carcinoma	0.1530	±	0.1466	14.6790	±	2.9980	0.0804	±	0.1496	10.2200	±	0.6506	0.1265	±	0.1348	11.1920	±	0.5947	---	---	50% cancer with 50% fibrous tissue, fat at edges
26a	Infiltrating Carcinoma	0.2766	±	0.1083	38.0062	±	4.5528	0.1585	±	0.1562	26.6720	±	0.9332	0.2792	±	0.0119	30.2260	±	6.0249	71	high	60% of specimen, 10-20% fibrous tissue
26b	Infiltrating Carcinoma	0.1497	±	0.1277	19.5680	±	4.6343	0.0884	±	0.1570	19.2720	±	1.3197	-0.0103	±	0.1333	17.9930	±	2.0233	71	high	80% of specimen, 20% fibrous tissue
28	Infiltrating Carcinoma	0.1564	±	0.1909	13.9480	±	1.2488	0.1291	±	0.1492	14.4140	±	0.9898	0.1147	±	0.1316	14.5320	±	4.2270	67	high	60% of specimen, in cancer area 70% fibrous tissue
30a	Infiltrating Carcinoma	-0.0218	±	0.1983	9.7729	±	0.6904	-0.0451	±	0.1734	8.6466	±	0.4610	-0.0257	±	0.1797	8.5188	±	0.5722	49	---	not much cancer present
31a	Infiltrating Carcinoma	0.1269	±	0.1664	6.9169	±	0.3811	0.0286	±	0.1761	7.3415	±	0.6167	0.0424	±	0.1723	7.0584	±	0.3669	68	intermediate	Cancer in most of specimen, 80-90% connective tissue
32	Infiltrating Carcinoma	0.4702	±	0.2281	3.0356	±	1.3523	0.0480	±	0.1712	3.2207	±	0.4737	0.1098	±	0.1179	4.1759	±	1.3192	78	intermediate	Cancer present in entire specimen
33a	Infiltrating Carcinoma	-0.0230	±	0.1964	7.2651	±	0.5064	0.0258	±	0.1897	7.5330	±	0.4435	0.0554	±	0.1894	7.8803	±	0.8760	78	high	70% cancer cells, some fat on outside, some tumor necrosis
33b	Infiltrating Carcinoma	-0.0417	±	0.1907	8.2406	±	0.8305	0.0104	±	0.1845	9.1953	±	1.3562	0.0416	±	0.1805	10.4900	±	3.0975	78	high	Cancer present in entire specimen,
35	Infiltrating Carcinoma	0.3275	±	0.2569	8.6164	±	1.0042	0.0053	±	0.1865	9.5242	±	0.8243	-0.0223	±	0.1932	6.8038	±	0.0434	39	intermediate	80% of specimen, in cancer 30-40% cells with connective tissue
40	Infiltrating Carcinoma	0.1857	±	0.2006	5.8433	±	1.4400	-0.0977	±	0.1861	4.3690	±	0.7725	-0.1063	±	0.1660	3.6123	±	1.5867	48	high	90% of specimen, of cancer, 30% fat and 10% epithelial elements
47a	Infiltrating Carcinoma	-0.0502	±	0.1999	10.0136	±	0.8175	-0.0263	±	0.1887	8.5213	±	0.4607	-0.0023	±	0.1887	7.5041	±	0.1726	59	low-inter	Cancer in most of specimen, 80% of specimen dense fibrous tissue
47b	Infiltrating Carcinoma	-0.0145	±	0.1879	7.5368	±	0.2723	0.0123	±	0.1693	7.7680	±	0.5958	0.0164	±	0.1849	7.3775	±	0.1121	59	low-inter	Mostly cancer with 20-30% fat on outside of specimen
50	Infiltrating Carcinoma	-0.0378	±	0.1891	4.8030	±	0.4291	-0.0611	±	0.1785	5.1373	±	1.6205	-0.0627	±	0.1907	4.1204	±	0.2239	38	inter	Cancer in most of specimen, 60-70% cancer cells
52	Infiltrating Carcinoma	0.5127	±	0.1555	14.2358	±	1.1242	0.2444	±	0.1458	19.8770	±	9.1001	0.3918	±	0.1086	13.5340	±	4.0845	---	int-high	50% cancer, 50% fibrous tissue
53	Infiltrating Carcinoma	0.1312	±	0.1962	13.0520	±	1.6478	-0.0140	±	0.1781	13.1080	±	2.4288	0.0599	±	0.1880	13.3530	±	1.3741	---	---	70% cancer with fat and fibrous tissue mixed in
54a	Infiltrating Carcinoma	0.0434	±	0.1442	5.1030	±	0.3276	0.0023	±	0.1573	7.9662	±	1.4047	0.0914	±	0.1640	9.0842	±	1.3788	46	low-inter	30% cancer, 70% fibrous tissue
55	Infiltrating Carcinoma	-0.0084	±	0.1838	6.3399	±	0.7310	-0.1918	±	0.1918	23.3010	±	4.7089	0.0964	±	0.1878	8.5096	±	1.3316	43	low-inter	15% cancer, rest fibrous tissue
56	Infiltrating Carcinoma	-0.0279	±	0.1892	12.1420	±	0.7261	-0.0240	±	0.1831	13.8110	±	1.2109	-0.0359	±	0.1889	10.8480	±	0.9458	43	---	50% of specimen cancer, of specimen 70% fibrous tissue and 30% fat
61	Infiltrating Carcinoma	-0.0095	±	0.2029	11.7898	±	1.5391	-0.0253	±	0.1734	9.6683	±	0.6731	-0.0139	±	0.1796	8.7310	±	0.9545	---	high	80% of specimen
63a	Infiltrating Carcinoma	0.0149	±	0.1934	5.4254	±	0.5062	-0.0127	±	0.1728	4.8173	±	0.9281	-0.0173	±	0.1654	3.7958	±	0.7156	45	intermediate	80% of specimen
63b	Infiltrating Carcinoma	0.0955	±	0.1920	11.8130	±	0.3861	0.0735	±	0.1811	10.0140	±	1.0036	0.0577	±	0.1864	8.5132	±	0.3870	45	intermediate	80% of specimen, lymphocytes present (10%)
65	Infiltrating Carcinoma	0.0485	±	0.1927	13.6254	±	0.4421	0.0371	±	0.1898	10.2290	±	1.3590	0.0458	±	0.1801	9.4177	±	1.1848	---	---	Less than 5% cancer present, mostly dense connective tissue
70	Infiltrating Carcinoma	0.0941	±	0.2006	8.9565	±	0.0682	0.0811	±	0.1846	10.8020	±	2.2875	1.1972	±	1.3746	2.3544	±	6.3660	82	---	40% of specimen
75	Infiltrating Carcinoma	0.2890	±	0.1940	9.4452	±	1.0289	-0.0267	±	0.1894	5.0773	±	1.3499	-0.0269	±	0.1892	3.8662	±	1.0570	36	high	Lots of connective tissue present
76	Infiltrating Carcinoma	0.2519	±	0.1941	12.1087	±	1.1446	-0.0076	±	0.1842	10.3312	±	0.2258	-0.0254	±	0.1896	9.4068	±	0.8472	43	high	40-50% cancer mixed with fat
78	Infiltrating Carcinoma	0.4611	±	0.1724	13.5586	±	1.6076	0.0551	±	0.1760	11.2743	±	1.4816	0.0540	±	0.1707	11.7452	±	1.5136	59	---	---
79	Infiltrating Carcinoma	0.3812	±	0.1912	7.2031	±	0.6305	0.0573	±	0.1685	6.7161	±	0.1461	0.0543	±	0.1854	6.9196	±	0.3975	45	intermediate	40% of specimen
81	Infiltrating Carcinoma	0.3118	±	0.1605	6.6185	±	4.6801	-0.0404	±	0.1812	3.3601	±	0.1348	0.1560	±	0.1355	7.2097	±	0.4811	73	intermediate	50% of specimen, tiny bit of fat
82	Infiltrating Carcinoma	0.1757	±	0.2001	5.7712	±	1.0750	-0.0482	±	0.1889	5.9825	±	0.2557	-0.0210	±	0.1839	5.5933	±	0.4695	---	---	60% of specimen
83	Infiltrating Carcinoma	0.2335	±	0.1980	10.7881	±	0.4201	0.0510	±	0.1817	7.6854	±	0.8023	0.1785	±	0.1903	7.9786	±	0.8275	52	high	20% cancer, 25% fat, 10% connective tissue rest dense fibrous tissue
84	Infiltrating Carcinoma	0.2969	±	0.1725	13.9281	±	0.5783	0.1256	±	0.1771	12.8880	±	0.2327	0.2400	±	0.1878	9.9301	±	0.3391	62	intermediate	60% of specimen, tumor necrosis
85	Infiltrating Carcinoma	0.1887	±	0.2007	7.2346	±	1.8555	0.0260	±	0.1683	4.5759	±	1.2348	0.1428	±	0.1492	4.1555	±	1.2078	73	high	50% of specimen
87	Infiltrating Carcinoma	0.0519	±	0.1976	21.8716	±	4.7607	0.1446	±	0.1602	20.4966	±	4.2048	0.0467	±	0.1726	14.4202	±	0.0162	69	high	25% cancer, 10% fat rest dense connective tissue
88a	Infiltrating Carcinoma	0.2501	±	0.1841	7.8824	±	1.8103	0.1440	±	0.0462	5.7492	±	4.6022	0.1147	±	0.1625	8.1515	±	1.5817	---	---	small edge with cancer, rest dense scar tissue, outside fat
88b	Infiltrating Carcinoma	0.2348	±	0.1791	5.9113	±	0.7447	0.2513	±	0.1613	5.8636	±	0.4951	0.1858	±	0.1770	4.5991	±	0.3876	---	---	90% dense scar tissue
42	Mucinous cancer	0.1345	±	0.1214	9.5740	±	4.6341	0.0974	±	0.1287	8.2375	±	2.7758	0.1214	±	0.1353	9.8570	±	1.9205	66	---	60% of specimen mucinous, 20% fibrous tissue
64	Mucinous cancer	0.1047	±	0.1553	4.0442	±	0.8701	0.0290	±	0.1750	4.6733	±	1.2326	0.0759	±	0.1395	3.1351	±	1.0206	---	---	Cancer mixed with fat
72	Mucinous cancer	0.5385	±	0.1882	4.8274	±	0.3647	-0.0775	±	0.1279	2.3553	±	1.2172	-0.1267	±	0.1844	1.3348	±	0.0582	---	---	Mucinous carcinoma with fat and muscle
3a	DCIS	0.0334	±	0.1552	8.6888	±	1.7607	-0.0215	±	0.1882	8.7878	±	0.1407	-0.0210	±	3.9682	7.6561	±	1.0678	72	---	Cancer with fat and connective tissue in entire specimen
3b	DCIS	0.0882	±	0.1963	16.4794	±	0.7440	0.0754	±	0.1873	15.2285	±	1.1697	0.0780	±	2.1373	14.9369	±	0.5982	72	---	50% of sample carcimoma, fat around outside
86	DCIS	0.2046	±	0.1823	11.0134	±	1.1541	0.0448	±	0.1752	11.2002	±	1.6949	0.1518	±	0.1777	8.0455	±	1.6236	---	---	carcinoma with dense connective tissue
62c	DCIS	0.0221	±	0.1524	14.1866	±	1.1639	0.0005	±	0.1846	11.0061	±	0.5349	-0.0273	±	0.1823	10.0810	±	1.0442	64	---	cancer present in one corner
62d	DCIS	0.0331	±	0.1939	15.1640	±	0.6239	0.0179	±	0.1730	14.8048	±	2.0886	0.0113	±	0.1746	11.5736	±	1.1683	64	---	ducts with cancer present, 5% hyperplasia in specimen
4	fibrous	0.1198	±	0.1684	5.9109	±	1.0447	0.1006	±	0.1285	5.6390	±	1.5082	0.0802	±	3.3817	5.9137	±	0.9173	70	---	50% fibrous tissue, 5% glands and ducts
7b	fibrous	0.3317	±	0.1202	11.8053	±	4.3243	0.3390	±	0.1107	9.0518	±	1.7866	0.2798	±	0.1189	10.8995	±	2.6037	60	---	50% fibrous tissue with benign atrophic ducts
9	fibrous	0.1119	±	0.1722	10.5050	±	0.4748	0.1206	±	0.1683	10.2610	±	0.8034	0.0914	±	0.1723	9.8415	±	0.5415	48	---	75% fibrous tissue, 15% fat, 10% normal
10	fibrous	0.3630	±	0.0306	13.7710	±	1.9906	0.3677	±	0.1716	12.0020	±	1.2265	0.3188	±	0.1254	10.1140	±	1.4254	54	---	60% fibrous tissue, 20% epithelial, 20% fat
11	fibrous	0.1595	±	0.1957	6.8397	±	0.7013	0.1346	±	0.1691	7.8452	±	1.3554	0.0225	±	0.1635	4.7626	±	0.2311	57	---	5% fibrous tissue
15	fibrous	0.0510	±	0.1933	10.8410	±	3.0769	0.0427	±	0.1831	9.5942	±	4.0183	0.1222	±	0.1636	8.0360	±	0.9612	35	---	35% fibrous, 60% fat, 5% benign
27	fibrous	0.1143	±	0.1719	12.0630	±	1.6071	0.0507	±	0.1794	11.3760	±	1.2264	0.0231	±	0.1840	9.0806	±	0.2149	40	---	60% fibrous, 10% benign epithelium
30b	fibrous	-0.0185	±	0.1931	9.2388	±	1.2032	-0.0608	±	0.1806	7.9748	±	0.5853	-0.0256	±	0.1618	6.9890	±	1.1147	49	---	60% fibrous tissue, little fat at outer edge, 40% benign breast
30c	fibrous	0.0173	±	0.1891	10.6461	±	0.7103	0.4352	±	0.3041	8.6702	±	0.8464	0.1028	±	0.1642	8.6509	±	0.9017	49	---	60% fibrous tissue, little fat at outer edge, 40% benign breast
34a	fibrous	0.0559	±	0.1870	4.7789	±	0.7287	0.1027	±	0.1527	6.0909	±	0.5879	0.1121	±	0.1819	7.2995	±	0.8755	51	---	70% fibrous tissue, 10% glands, 20% fat
34b	fibrous	0.4193	±	0.4572	7.4609	±	1.9427	0.0039	±	0.1694	7.9001	±	1.3276	0.0342	±	0.1734	8.4212	±	1.6793	51	---	70% fibrous tissue, 10% glands, 20% fat
36	fibrous	-0.0266	±	0.1990	13.9990	±	0.0584	-0.0296	±	0.1890	13.4810	±	1.7909	-0.0302	±	0.1907	10.1370	±	0.2430	29	---	80% fibrous tissue, 20% fat
37	fibrous	0.0686	±	0.1911	6.5724	±	0.3406	0.0820	±	0.1820	5.1981	±	0.1469	0.0690	±	0.1718	5.6339	±	0.2152	---	---	---
39	fibrous	0.3022	±	0.1817	10.0180	±	1.3536	-0.0351	±	0.1836	7.8963	±	1.0984	-0.0511	±	0.1716	5.5508	±	2.2367	73	---	60% fibrous, 30% fat, 10% epithelial

Table 2 (Continued).

		λ = 749 nm				λ = 789 nm				λ = 836 nm						
Sample	Type	μ_a(cm^{-1})*		μ_s'(cm^{-1})		μ_a(cm^{-1})*		μ_s'(cm^{-1})		μ_a(cm^{-1})*		μ_s'(cm^{-1})		AGE	Grade	Comments
41	fibrous	0.2941 ±	0.1979	6.9392 ±	0.2541	-0.0919 ±	0.1692	4.3152 ±	0.8880	-0.0618 ±	0.1758	4.7319 ±	0.7217	69	---	20% fibrous tissue, some fat
43	fibrous	0.0424 ±	0.1924	12.1190 ±	0.4397	-0.0135 ±	0.1855	9.9358 ±	1.1350	0.0168 ±	0.1910	10.8374 ±	0.6894	---	---	50% fibrous tissue and fat, 10-20% ducts in fibrous tissue
44a	fibrous	0.0050 ±	0.1831	13.3042 ±	1.6504	-0.0013 ±	0.1747	11.5217 ±	0.4596	0.0042 ±	0.1671	11.0265 ±	1.4716	59	---	fibrous tissue with fat
44b	fibrous	0.0884 ±	0.1921	13.1426 ±	0.6117	0.0594 ±	0.1764	12.7912 ±	1.8448	0.0772 ±	0.1757	12.7695 ±	1.5954	59	---	fibrous tissue with fat
45a	fibrous	0.0032 ±	0.1982	13.1202 ±	0.5491	-0.0048 ±	0.1841	12.2936 ±	0.5634	0.0177 ±	0.1768	10.6467 ±	1.5486	50	---	80% fibrous, 10% fat, 10% glands
45b	fibrous	-0.0211 ±	0.1980	10.5704 ±	1.3677	-0.0362 ±	0.1852	10.3285 ±	2.0598	0.0099 ±	0.1853	8.7234 ±	1.4264	50	---	80% fibrous, 10% fat, 10% glands
46a	fibrous	0.0139 ±	0.1975	10.9489 ±	3.6771	0.0045 ±	0.1772	9.3028 ±	2.6897	0.0482 ±	0.1674	11.1347 ±	1.7276	44	---	50% fibrous tissue, 50% fat, some hyperplasia
46b	fibrous	0.0152 ±	0.1892	9.5271 ±	2.1868	0.0025 ±	0.1848	8.9343 ±	1.3873	0.0416 ±	0.1713	9.8990 ±	0.5842	44	---	50% fibrous tissue, 50% fat
47c	fibrous	0.1683 ±	0.1924	4.8698 ±	0.5953	0.1210 ±	0.1710	5.2128 ±	0.5359	0.1530 ±	0.1717	5.9967 ±	1.4157	59	---	20% fibrous
47d	fibrous	0.0532 ±	0.2014	5.9405 ±	1.1875	0.0570 ±	0.1885	5.8476 ±	1.1245	0.0683 ±	0.1871	5.9520 ±	2.2828	59	---	50% fibrous, 50% fat
48	fibrous	0.0286 ±	0.2028	11.7207 ±	0.5982	-0.0150 ±	0.1906	11.7550 ±	0.9006	-0.0310 ±	0.1348	8.2505 ±	1.8478	64	---	80% fibrous, 20% fat
59a	fibrous	0.0218 ±	0.1849	12.1588 ±	0.9116	-0.0260 ±	0.1774	11.9516 ±	0.7793	-0.0043 ±	0.1653	7.8951 ±	0.6314	16	---	65% fibrous tissue, 30% fat, 5% epithelium
59b	fibrous	0.0591 ±	0.1932	10.3538 ±	1.5123	0.0366 ±	0.1684	10.2179 ±	1.2956	0.0227 ±	0.1940	7.9944 ±	0.0095	16	---	65% fibrous tissue, 30% fat, 5% epithelium
60a	fibrous	-0.0195 ±	0.1898	9.7566 ±	0.8090	-0.0271 ±	0.1801	10.0048 ±	1.3833	-0.0243 ±	0.1787	8.4943 ±	0.7019	24	---	50% fibrous, 20% fat
60b	fibrous	-0.0238 ±	0.1906	13.0317 ±	2.0576	-0.0379 ±	0.1815	10.3237 ±	1.0593	-0.0406 ±	0.1879	9.4029 ±	1.0035	24	---	50% fibrous, 20% fat
62a	fibrous	0.0343 ±	0.2016	9.6335 ±	1.7335	-0.0284 ±	0.1804	10.3951 ±	2.1742	-0.0245 ±	0.1775	8.2817 ±	1.8964	64	---	Mostly fibrous, 20% fat
62b	fibrous	0.0706 ±	0.1694	8.3035 ±	0.5545	0.0559 ±	0.1766	8.1649 ±	1.0043	0.0226 ±	0.1759	6.1467 ±	0.9455	64	---	Mostly fibrous, 20% fat
66	fibrous	0.0517 ±	0.1907	5.4748 ±	0.4045	0.0287 ±	0.1855	5.4733 ±	0.0688	0.0306 ±	0.1907	3.8866 ±	0.2275	16	---	fibroadenoma
67	fibrous	0.1115 ±	0.1841	7.6569 ±	0.7736	0.0640 ±	0.1801	6.8821 ±	1.2744	0.0528 ±	0.1910	4.5165 ±	0.5109	22	---	fibrous tissue and fat
74	fibrous	0.5098 ±	0.1865	10.1849 ±	0.1214	0.0921 ±	0.1862	8.0615 ±	0.9356	0.0650 ±	0.1873	8.3018 ±	0.4663	77	---	fibrous and fat
80	fibrous	0.8639 ±	0.0239	7.9294 ±	2.2466	0.2205 ±	0.1065	6.3801 ±	0.5962	0.1531 ±	0.1342	7.1246 ±	1.0158	40	---	fibrous tissue and fat
12	fatty	0.1181 ±	0.2008	10.4600 ±	2.5841	0.0704 ±	0.1632	12.0780 ±	2.8071	0.2156 ±	0.1653	9.7426 ±	1.0783	63	---	60% fat rest fibrous tissue
14	fatty	0.0414 ±	0.1837	3.7537 ±	0.8048	0.0519 ±	0.1906	4.4437 ±	0.7236	0.1074 ±	0.1812	5.2875 ±	0.4425	67	---	mostly fat with tiny cysts
17	fatty	0.3919 ±	0.1698	12.4101 ±	1.6392	0.3153 ±	0.1036	12.2570 ±	1.2205	0.2335 ±	0.1500	12.1060 ±	2.5209	56	---	60% fat with 40% fibrous tissue
18	fatty	0.1716 ±	0.1905	15.5870 ±	0.5115	0.1112 ±	0.1754	13.2120 ±	0.8680	0.1887 ±	0.1746	10.9300 ±	1.0870	58	---	fat with strands of fibrous tissue
19	fatty	0.1776 ±	0.1609	10.9620 ±	1.1542	0.0822 ±	0.1666	9.9369 ±	3.0303	0.1532 ±	0.1828	12.0400 ±	0.5136	43	---	fat with strands of fibrous tissue
20	fatty	0.1374 ±	0.1580	9.2487 ±	0.2956	0.0395 ±	0.1721	8.1791 ±	0.4126	0.0690 ±	0.1573	9.4531 ±	1.0116	74	---	fat with 20% fibrous tissue
21	fatty	0.2803 ±	0.1565	7.9530 ±	1.7892	0.1339 ±	0.1534	6.5053 ±	0.5746	0.1570 ±	0.1712	6.8338 ±	0.3336	27	---	all fat
25a	fatty	0.3050 ±	0.1293	7.2374 ±	1.5952	0.3528 ±	0.0917	7.0227 ±	1.0852	0.1988 ±	0.1088	6.4883 ±	0.7752	30	---	predominantly fatty with streaks of fibrous tissue
25b	fatty	0.1805 ±	0.1135	8.6552 ±	3.3608	0.0793 ±	0.1861	6.7230 ±	2.3343	0.1161 ±	0.1811	5.1472 ±	1.1840	30	---	predominantly fatty with streaks of fibrous tissue
25c	fatty	0.3360 ±	0.1550	6.6181 ±	0.3671	0.2601 ±	0.1181	6.0318 ±	0.7819	0.3039 ±	0.1597	7.5846 ±	0.9904	30	---	predominantly fatty with streaks of fibrous tissue
25d	fatty	0.2238 ±	0.0978	7.3269 ±	0.6749	0.1489 ±	0.1287	7.2633 ±	0.2364	0.1947 ±	0.1666	7.1060 ±	1.7812	30	---	predominantly fatty with streaks of fibrous tissue
31b	fatty	0.1194 ±	0.1878	5.2241 ±	0.6049	0.0885 ±	0.1779	7.0244 ±	2.1473	0.0723 ±	0.1917	4.4489 ±	0.3386	68	---	80% fat, 20% fibrous tissue
31c	fatty	0.1343 ±	0.1625	7.3344 ±	1.8692	0.1087 ±	0.1748	7.1627 ±	0.8763	0.1793 ±	0.1787	6.0450 ±	1.0819	68	---	80% fat, 20% fibrous tissue
38a	fatty	0.0572 ±	0.2015	12.7514 ±	2.9613	-0.0069 ±	0.1814	8.4934 ±	2.1477	0.0140 ±	0.1811	7.0560 ±	1.0574	42	---	70-80% fat, rest fibrous
38b	fatty	0.3665 ±	0.1766	11.3410 ±	1.5572	-0.0424 ±	0.1810	9.3001 ±	1.2541	-0.0204 ±	0.1860	9.9423 ±	1.3866	42	---	70-80% fat, rest fibrous
49a	fatty	0.0004 ±	0.1921	4.5054 ±	1.0622	-0.0412 ±	0.1805	4.0278 ±	0.7086	-0.0291 ±	0.1772	3.6257 ±	1.2174	26	---	mostly fat, 20% fibrous tissue
49b	fatty	0.0166 ±	0.2024	4.0621 ±	0.2981	-0.0366 ±	0.1758	3.8916 ±	0.6868	-0.0230 ±	0.1893	3.9649 ±	0.0689	26	---	mostly fat, 20% fibrous tissue
54b	fatty	0.0241 ±	0.2005	4.4436 ±	0.1507	0.0392 ±	0.1853	4.9459 ±	0.1601	0.2164 ±	0.0272	4.6211 ±	0.4871	46	---	mostly fat, 20% fibrous tissue, 10% glands
68	fatty	0.0338 ±	0.1888	4.3421 ±	0.3666	0.0197 ±	0.1823	4.5765 ±	0.6785	0.0676 ±	0.1770	6.2487 ±	0.1986	---	---	mostly fat with area of fibrous tissue
69	fatty	0.0339 ±	0.1584	10.0184 ±	0.7278	-0.0485 ±	0.1910	9.7421 ±	0.1446	-0.0465 ±	0.1888	7.2343 ±	1.5106	---	---	40% fat, 10% epithelial
71	fatty	0.0184 ±	0.1940	7.6501 ±	1.3615	0.0148 ±	0.1883	8.0893 ±	0.4313	-0.0088 ±	0.1839	6.2038 ±	0.9768	---	---	lots of tissue with fat
73	fatty	0.5930 ±	0.1830	15.7746 ±	1.5642	0.0685 ±	0.1887	9.5180 ±	1.3508	0.0461 ±	0.1653	6.4803 ±	1.3011	71	---	mostly fat
77	fatty	0.4663 ±	0.1735	7.3079 ±	1.3426	0.0728 ±	0.1650	6.0507 ±	1.2934	0.0704 ±	0.1856	8.7090 ±	0.0709	---	---	mostly fat with areas of collagen
64b	skin	0.2428 ±	0.1920	0.7530 ±	23.1405	0.7530 ±	0.0632	22.7586 ±	1.2943	0.9767 ±	0.1522	15.9443 ±	2.1584	---	---	skin

*Negative values of absorption coefficient are small and obtained after the correlations have been made. μ_a values are within the error of the measurement.

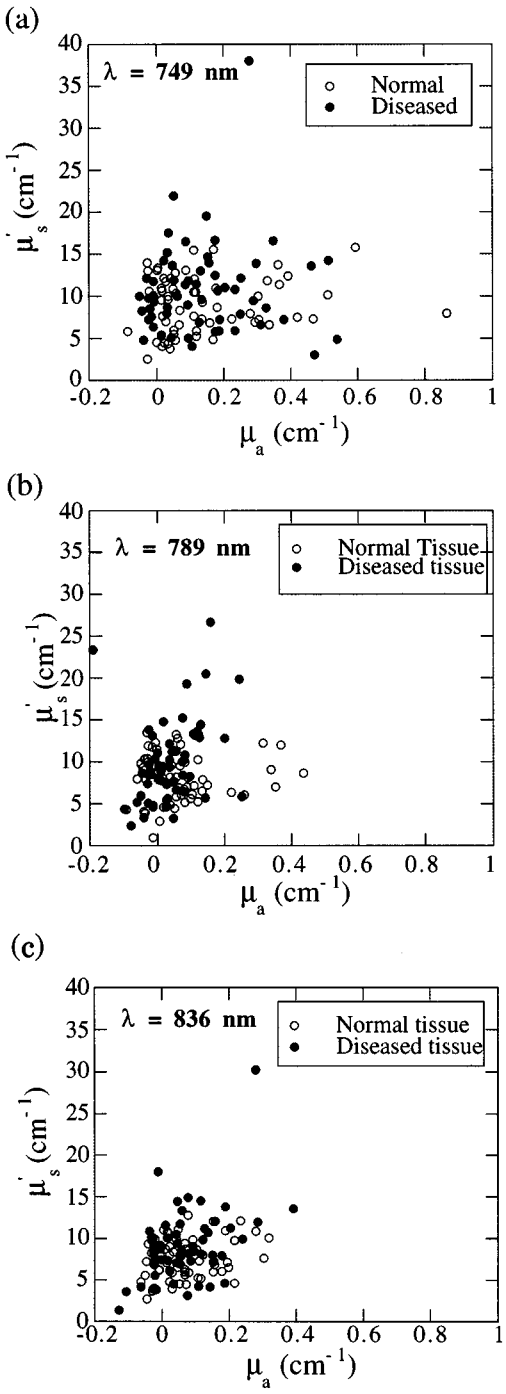

Fig. 5 Experimental optical properties of normal and diseased breast tissues reported as the isotropic scattering coefficient μ'_s versus the absorption coefficient μ_a measured at (a) 749, (b) 789, and (c) 836 nm where the open circles represent normal tissues and the closed circles represent diseased tissues.

between the scattering coefficients of ductal carcinoma *in situ* and normal fatty tissues. However, trends do exist. Infiltrating carcinoma and ductal carcinoma *in situ* have the highest scattering properties at each of the three wavelengths. This result is inconsistent with Peters et al.,[25] who report that cancerous tissues have lower scattering properties than fibrous tissue types.

In all tissue classifications, there are no observable trends of absorption coefficient with histopathology. Since tissue measurements are made *in vitro*, again it is unlikely that these measurements will accurately reflect the blood volume and hence the contrast due to absorption *in vivo*. However, Peters et al.[25] found that tissues with varying pathologies have differing absorbances, with carcinomas having the highest value of μ_a.

4 EXPERIMENTAL MEASUREMENTS PREDICTING μ_A AND $\mu_{S'}$ OF NORMAL AND DISEASED BREAST TISSUES FROM THE SAME PATIENT

From Figures 5(a) though 5(c) presented earlier, there is no consistent optical contrast provided between normal and diseased tissues pooled from 88 patients. In five tissue specimens, tissue volumes were significant, enabling optical property measurement of diseased and surrounding normal tissues. Table 4 lists the tissue optical properties for normal and diseased tissues for five patients with histological pathologies of (1) normal fibrous/ductal carcinoma *in situ*, (2) normal fibrous/infiltrating carcinoma, (3) normal fatty/infiltrating carcinoma, and (4) normal skin/mucinous carcinoma. In the last specimen, skin tissue was inadvertently sampled, as evidenced by histopathology. Interestingly, the scattering coefficient of skin is higher than normal fatty and fibrous tissues, which is in agreement with literature reports.[28] The scattering coefficient of the mucinous tissue is low, which again is consistent with the pathology of the disease (see Sec. 2.4). While the number of measurements is small (due to the size of tissue samples), preventing statistical analysis, our results are nonetheless consistent in that the scattering coefficients of infiltrating carcinoma and ductal carcinoma *in situ* tissues are larger than the surrounding normal tissues, whether fatty or fibrous in nature. There appears to be no trend in the measured absorption coefficient, again probably due to the drainage of blood.

Recently, Gandjbakhche and co-workers[29] found that a significant difference in measured *in vitro* scattering coefficients at 633 and 800 nm exists between fatty normal tissue and adenocarcinoma tissue specimens from one patient. Their results show a doubling of scattering coefficient between the fatty and adenocarcinoma tissue specimens, which is consistent with the increased scattering between normal and diseased tissues that we found in our study (with the exception of the patient with mucinous carcinoma). Their results show a reduction in absorption with disease, a trend that was not evident in our study.

Table 3 Measured optical properties of classified breast tissue reported as the mean ± the standard deviation of the mean at 749, 789, and 836 nm.

	λ=749 nm		λ=789 nm		λ=836 nm	
	μ_a (cm^{-1})	μ_s' (cm^{-1})	μ_a (cm^{-1})	μ_s' (cm^{-1})	μ_a (cm^{-1})	μ_s' (cm^{-1})
Infiltrating carcinoma (*n*=48)	0.1474 ±0.1438	10.9139 ±5.5943	0.0443 ±0.0830	10.1253 ±5.0479	0.1000 ±0.1877	9.0969 ±4.5360
Mucinous carcinoma (*n*=3)	0.2592 ±0.1979	6.1485 ±2.4432	0.0163 ±0.0720	5.0887 ±2.4193	0.0235 ±0.1078	4.7756 ±3.6674
Ductal carcinoma *in situ* (*n*=5)	0.0763 ±0.0682	13.1065 ±2.8521	0.0234 ±0.0339	12.2055 ±2.4505	0.0386 ±0.0678	10.4586 ±2.6502
Fatty normal (*n*=23)	0.1838 ±0.1590	8.4768 ±3.4283	0.0818 ±0.1045	7.6728 ±2.5670	0.1077 ±0.0973	7.2739 ±2.4003
Fibrous normal (*n*=35)	0.1269 ±0.1866	9.7468 ±2.2704	0.0604 ±0.1193	8.9450 ±2.4502	0.0499 ±0.0832	8.0995 ±2.20704

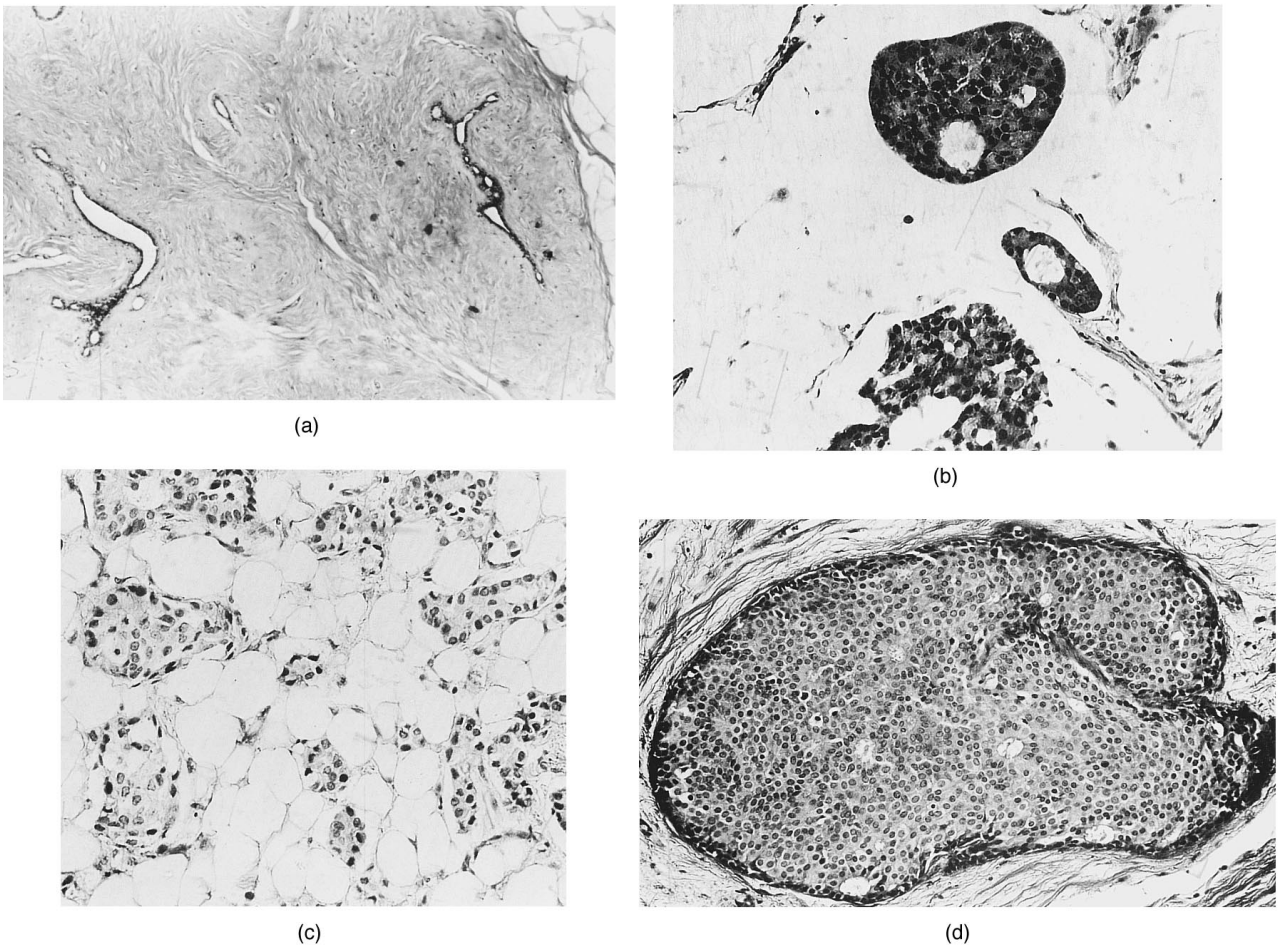

Fig. 6 (a) Micrograph of fibrous breast tissue with a fatty section in the upper right corner (×80). Reproduced from Ref. 35. (b) Micrograph of breast tissue with mucinous carcinoma (×225). Reproduced from Ref. 35. (c) Micrograph of low-grade infiltrating carcinoma with tubule formation. The sharp clear spaces are fat (×225). Reproduced from Reference 35. (d) Micrograph of ductal carcinoma *in situ* found in the breast (×225). Reproduced from Ref. 35.

Table 4 Optical properties of normal and diseased human breast tissue samples from the same patient at wavelengths of 749, 789, and 836 nm.

Sample	Type	λ = 749 nm		λ = 789 nm		λ = 836 nm		AGE	Grade	Comments
		μ_a (cm^{-1})	μ_s' (cm^{-1})	μ_a (cm^{-1})	μ_s' (cm^{-1})	μ_a (cm^{-1})	μ_s' (cm^{-1})			
30a	Infiltrating Carcinoma	-0.0218 ± 0.1983	9.7729 ± 0.6904	-0.0451 ± 0.1734	8.6466 ± 0.4610	-0.0257 ± 0.1797	8.5188 ± 0.5722	49	---	not much cancer present
30b	fibrous	-0.0185 ± 0.1931	9.2388 ± 1.2032	-0.0608 ± 0.1806	7.9748 ± 0.5853	-0.0256 ± 0.1618	6.9890 ± 1.1147	49	---	60% fibrous tissue, little fat at outer edge, 40% benign breast
30c	fibrous	0.0173 ± 0.1891	10.6461 ± 0.7103	0.4352 ± 0.3041	8.6702 ± 0.8464	0.1028 ± 0.1642	8.6509 ± 0.9017	49	---	60% fibrous tissue, little fat at outer edge, 40% benign breast
31a	Infiltrating Carcinoma	0.1269 ± 0.1664	6.9169 ± 0.3811	0.0286 ± 0.1761	7.3415 ± 0.6167	0.0424 ± 0.1723	7.0584 ± 0.3669	68	inter	Cancer in most of specimen, 80-90% connective tissue
31b	fatty	0.1194 ± 0.1878	5.2241 ± 0.6049	0.0885 ± 0.1779	7.0244 ± 2.1473	0.0723 ± 0.1917	4.4489 ± 0.3386	68	---	80% fat, 20% fibrous tissue
31c	fatty	0.1343 ± 0.1625	7.3344 ± 1.8692	0.1087 ± 0.1748	7.1627 ± 0.8763	0.1793 ± 0.1787	6.0450 ± 1.0819	68	---	80% fat, 20% fibrous tissue
47a	Infiltrating Carcinoma	-0.0502 ± 0.1999	10.0136 ± 0.8175	-0.0263 ± 0.1887	8.5213 ± 0.4607	-0.0023 ± 0.1887	7.5041 ± 0.1726	59	low-inter	Cancer in most of specimen, 80% of specimen dense fibrous tissue
47b	Infiltrating Carcinoma	-0.0145 ± 0.1879	7.5368 ± 0.2723	0.0123 ± 0.1693	7.7680 ± 0.5958	0.0164 ± 0.1849	7.3775 ± 0.1121	59	low-inter	Mostly cancer with 20-30% fat on outside of specimen
47c	fibrous	0.1683 ± 0.1924	4.8698 ± 0.5953	0.1210 ± 0.1710	5.2128 ± 0.5359	0.1530 ± 0.1717	5.9967 ± 1.4157	59	---	20% fibrous
47d	fibrous	0.0532 ± 0.2014	5.9405 ± 1.1875	0.0570 ± 0.1885	5.8476 ± 1.1245	0.0683 ± 0.1871	5.9520 ± 2.2828	59	---	50% fibrous, 50% fat
62a	fibrous	0.0343 ± 0.2016	9.6335 ± 1.7335	-0.0284 ± 0.1804	10.3951 ± 2.1742	-0.0245 ± 0.1775	8.2817 ± 1.8964	64	---	Mostly fibrous, 20% fat
62b	fibrous	0.0706 ± 0.1694	8.3035 ± 0.5545	0.0559 ± 0.1766	8.1649 ± 1.0043	0.0226 ± 0.1759	6.1467 ± 0.9455	64	---	Mostly fibrous, 20% fat
62c	DCIS	0.0221 ± 0.1524	14.1866 ± 1.1639	0.0005 ± 0.1846	11.0061 ± 0.5349	-0.0273 ± 0.1823	10.0810 ± 1.0442	64	---	cancer present in one corner
62d	DCIS	0.0331 ± 0.1939	15.1640 ± 0.6239	0.0179 ± 0.1730	14.8048 ± 2.0886	0.0113 ± 0.1746	11.5736 ± 1.1683	64	---	ducts with cancer present, 5% hyperplasia in specimen
64	Mucinous cancer	0.1047 ± 0.1553	4.0442 ± 0.8701	0.0290 ± 0.1750	4.6733 ± 1.2326	0.0759 ± 0.1395	3.1351 ± 1.0206	---	---	Cancer mixed with fat
64b	skin	0.2428 ± 0.1920	0.7530 ± 23.1405	0.7530 ± 0.0632	22.7586 ± 1.2943	0.9767 ± 0.1522	15.9443 ± 2.1584	---	---	skin

*Negative values of absorption coefficient are small and obtained after the corrections have been made (see text).

5 CONTRAST FOR PHOTON MIGRATION IMAGING

The success of optical breast cancer screening depends crucially upon detecting the presence of diseased breast tissues from surface measurements of photon migration. Time-dependent measurements of photon migration can be made in one of two ways: in the time and frequency domains. In the time domain, an incident impulse of light is launched into the tissue. As the pulse propagates through the tissues, its migration and attenuation are influenced by local tissue optical properties. The broadened, reemitted pulse provides information about the scattering medium through which it has propagated. In the frequency domain, a photon density wave is launched into the tissue. As the wave of photons propagates, it is attenuated and phase shifted with respect to the incident wave due to the local tissue optical properties. These measurements provide input into inverse imaging algorithms for image reconstruction or can be used directly to reconstruct tomographic images. Yet the question remains: Are the optical property differences between normal and diseased tissues significant enough to distort these measurements of photon migration and provide detection of breast cancer?

In order to answer this question, we solved the forward-imaging problem to detect changes in photon migration measurements in which a simulated diseased tissue volume was located in an otherwise homogeneous medium. The optical properties of the 70-mm diameter homogeneous medium were chosen to be identical to those measured at 749 nm for the fibrous normal tissues of patient 62 in Table 4. A 5-mm diameter diseased tissue volume with optical properties identical to those measured for the ductal carcinoma *in situ* in the same patient was embedded in the simulated tissue. While the high resolution for x-ray mammography is based largely upon the detection of calcifications, the minimal detectable volume for diseased tissues using optical tomography is not yet clear. Thus we arbitrarily choose to investigate optical tomography on a 5 mm tumor embedded in normal tissue. The diffusion equation that describes the local light propagation in tissues was solved in the time domain using commercial finite-element software (Fluid Dynamics International, Evanston, Illinois):

$$\frac{1}{c}\frac{\partial}{\partial t}\Phi(r,t) - D\nabla^2\Phi(r,t) + \mu_a\Phi(r,t) = S(r,t). \tag{2}$$

In Eq. (2), c is the speed of light in the medium (cm/s), Φ is the photon fluence rate (number of photons/cm^2 sec) at position r and time t, D is the optical diffusion coefficient (cm), which is defined as

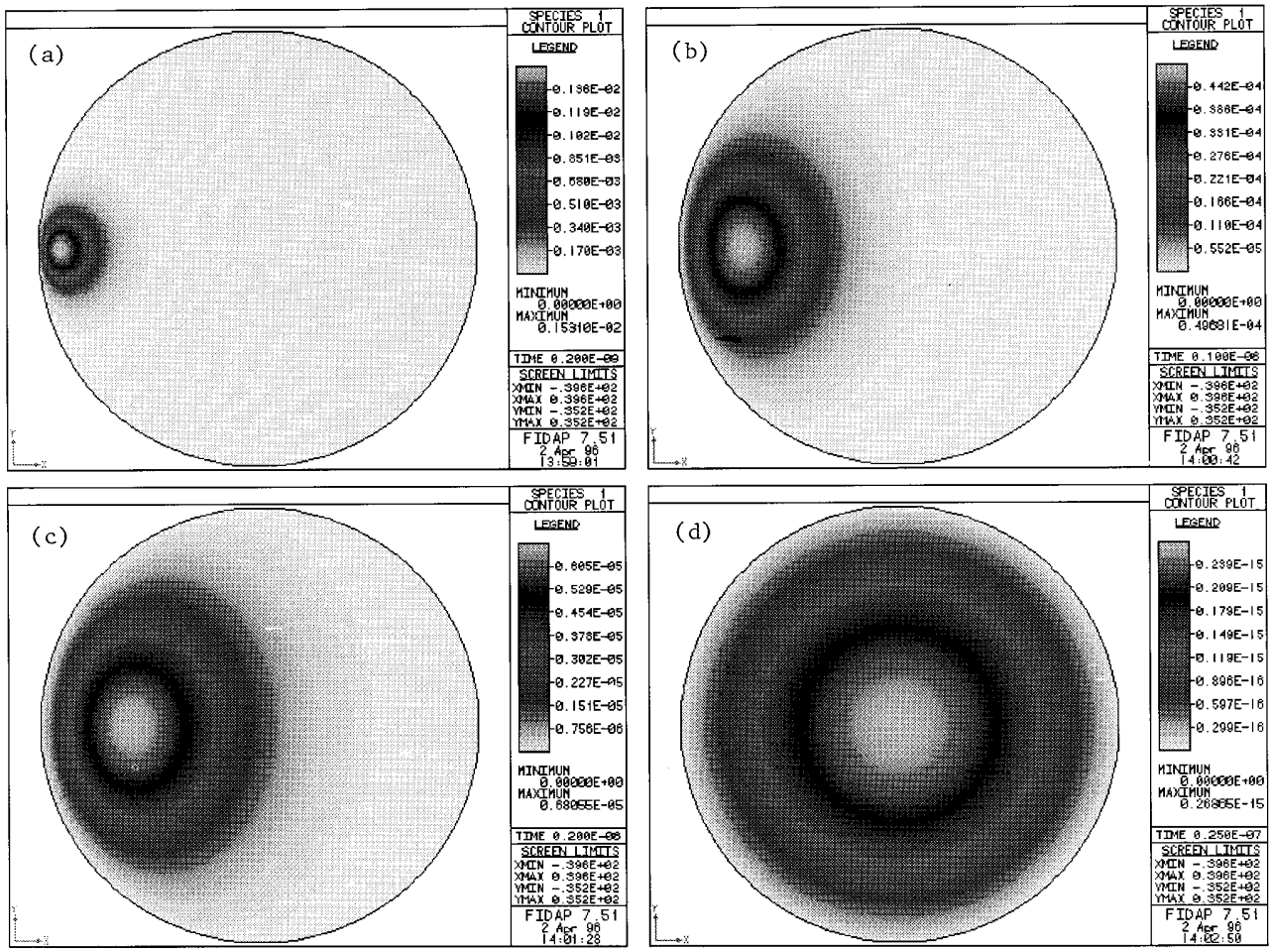

Fig. 7 Contour plots of the spatial distribution of light at (a) 0.2, (b) 1, (c) 2, and (d) 25 ns in a heterogeneous phantom after an initial impulse. The heterogeneity (0.5 cm in diameter) represents ductal carcinoma *in situ* tissue that is located 0.93 cm from the left edge.

$$D = \frac{1}{(3\mu_a + \mu'_s)}, \tag{3}$$

and S is the source term (number of photons/cm^3 sec). Since computations were prohibitive in three dimensions, we accounted for the two-dimensionality of our simulation by noting that a scattering length in two dimensions has $(3/2)^{1/2}$ (Ref. 30) the length of a three-dimensional scattering length. These simulations therefore mimic detection of a 5 mm cylindrical diseased volume. Four different meshes consisting of approximately 1700 quadrilateral elements with 7000 nodes were constructed. At a node located one scattering length beneath the surface, an initial condition of finite fluence served to simulate the incident impulse of light. Zero fluence boundary conditions were imposed, allowing more rapid computation on a SunSparc 10 workstation. The error in our source location and zero boundary condition assumption is minimal compared with the results for partial current boundary conditions[31] with an initial condition employing a surface node.[32]

Figures 7(a) to 7(d) are contour plots showing the simulated light propagation through the 2-D circular tissue phantom at times of 0.2, 1, 2, and 25 ns after an initial impulse of light. The incident impulse is launched from a point source located at the left edge. As time progresses, the light pulse broadens and attenuates toward the center of the phantom due to symmetry. The presence of the tumor causes light to be ''trapped'' within the object because of multiple scattering events causing a higher intensity within the heterogeneity. From these results, one can see that the propagation of NIR light in tissue is influenced by the presence of diseased tissues with optical properties similar to what has been measured in this study. However, can this change in light propagation characteristics be measured noninvasively?

In order to answer this question, we used data from our time domain finite-element solution and converted it to frequency domain measurements of phase shift and amplitude modulation using the Fourier transform.[33] For a detector located at an arc

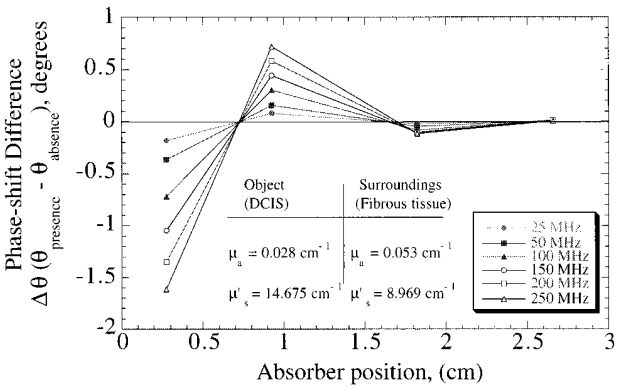

Fig. 8 Simulated phase-shift difference for a 0.5 cm diameter ductal carcinoma *in situ* heterogeneity in a 7 cm diameter normal tissue phantom as a function of object position away from the source and detector. Optical properties are taken from average values in Table 4 measured at 749 nm.

distance of 3.05 cm away from the source, we simulated the change in phase shift caused by the diseased tissue volume as a function of the modulation frequency and the position of the heterogeneity away from the tissue–air interface. Figure 8 shows the simulated phase-shift difference at frequencies of 25, 50, 100, 150, 200, and 250 MHz. This figure shows that the tumor causes an alteration in phase shift at depths of up to 1.8 cm at the measured frequencies. However, the maximum 2.3-degree change in phase shift may not be sufficient for detection. The presence of the heterogeneity can be determined at greater depths from lower frequencies and larger separations between the source and detector.[8]

6 CONCLUSIONS

Our results of optical property measurements of pooled tissue samples show that there are no statistical differences between normal and diseased tissues. However, these measurements underestimate absorption because of the blood drainage that occurs during excision. Therefore our measured absorption coefficients may not reflect the *in vivo* conditions. Since tumor angiogenesis may be responsible for increased vascularity and hemoglobin concentrations,[34] we expect our *in vitro* measurements to underestimate the contrast caused by absorption. Nevertheless, our data show an increased scattering coefficient in infiltrating and ductal carcinoma *in situ* tissues relative to fatty and fibrous tissues. Indeed, when diseased and normal tissues from the same patient are compared, significant differences in optical properties can be seen.

Acknowledgments

The authors gratefully acknowledge the assistance of Julia Smith, Will Nau, Thomas Wadsworth, and Lesley Likens. Appreciation goes to Scott Prahl for his assistance with the double integrating spheres and the use of his inverse adding-doubling algorithm, and Britton Chance and Murray Penney for their critical advice, suggestions and comments. This work was supported in part by the Whitaker Foundation and the National Institutes of Health (R01CA 61413, EMS).

REFERENCES

1. E. Marshall, ''Search for a killer: focus shifts from fat to hormones in a special report on breast cancer,'' *Science* **259**, 618–621 (1993).
2. R. J. Epstein, ''Does the breast cancer dollar make sense?'' *Eur. J. Cancer* **28**, 486–491 (1992).
3. J. R. Singer, F. A. Grumbaum, P. Kohn, and J. P. Zubelli, ''Image reconstruction of the interior of bodies that diffuse radiation,'' *Science* **248**, 990–993 (1990).
4. B. B. Das, K. M. Yoo, and R. R. Alfano, ''Ultrafast time-gated imaging in thick tissues: a step toward optical mammography,'' *Opt. Lett.* **18**, 1092–1094 (1993).
5. J. C. Hebden, R. A. Kruger, and K. S. Wong, ''Time resolved imaging through a highly scattering medium,'' *Appl. Opt.* **30**, 788–794 (1991).
6. D. A. Boas, M. A. O'Leary, B. Chance, and A. G. Yodh, ''Scattering of diffuse photon density waves by spherical inhomogeneities within turbid media: analytic solution and applications,'' *Proc. Natl. Acad. Sci. U.S.A.* **91**, 4887–4891 (1994).
7. H. Jiang, K. D. Paulsen, U. L. Osterberg, B. W. Pogue, and M. S. Patterson, ''Simultaneous reconstruction of absorption and scattering maps in turbid media from near-infrared frequency-domain data,'' *Opt. Lett.* **20**, 2128–2130 (1995).
8. E. M. Sevick, J. K. Frisoli, C. L. Burch, and J. R. Lakowicz, ''Localization of absorbers on scattering media using frequency domain measurements of time-dependent photon migration,'' *Appl. Opt.* **33**, 3562–3570 (1994).
9. B. W. Pogue, M. S. Patterson, H. Jiang, and K. D. Paulsen, ''Initial assessment of a simple system for frequency domain diffuse optical tomography,'' to appear in *Physics in Medicine and Biology* (1996).
10. R. L. Barbour, H. L. Graber, Y. Wang, J. H. Chang, and R. Aronson, ''A perturbation approach for optical diffusion tomography using continuous-wave and time resolved data,'' *Proc. SPIE* **IS11**, 87–120 (1993).
11. M. S. Patterson, B. C. Wilson, and B. Chance, ''Time-resolved reflectance and transmittance for non-invasive measurements of tissue optical properties,'' *Appl. Opt.* **28**, 2331–2336 (1989).
12. B. Beauvoit, S. M. Evans, T. W. Jenkins, E. E. Miller, and B. Chance, ''Correlation between the light scattering and the mitochondrial content of normal tissues and transplantable rodent tumors,'' *Anal. Biochem.* **226**, 167–174 (1995).
13. B. Chance, H. Liu, T. Kitai, and Y. Zhang, ''Effects of solutes on optical properties of biological materials: models, cells and tissues,'' *Anal. Biochem.* **227**, 351–362 (1995).
14. M. A. O'Leary, D. A. Boas, B. Chance, and A. G. Yodh, ''Experimental images of heterogeneous turbid media by frequency-domain diffusion-photon tomography,'' *Opt. Lett.* **20**, 426–428 (1995).
15. H. Jiang, ''Reconstructed near infrared diffusion imaging for breast cancer detection,'' Ph.D. diss., Dartmouth College, Hanover, NH (1995).
16. E. M. Sevick, J. R. Lakowicz, H. Szmacinski, K. Nowaczyk, and M. L. Johnson, ''Frequency domain imaging of absorbers obscured by scattering,'' *J. Photochem. Photobio, B:Biol* **16**, 169–185 (1992).
17. M. A. Franceschini, K. T. Moesta, S. Fantini, G. Gaida, E. Gratton, H. Jess, W. W. Mantulin, M. Seever, P. M. Schlag, and M. Kaschke, ''Frequency-domain instrumentation enhances optical mammography: initial clinical results,'' Proc. Natl. Acad. Sci. U.S.A. (submitted April 1996).
18. J. W. Pickering, S. A. Prahl, N. van Wieringen, J. F. Beek, H. J. Sterenborg, and M. J. van Gemert, ''Double-integrating-sphere system for measuring the optical properties of tissue,'' *Appl. Opt.* **32**, 399–410 (1993).

19. S. A. Prahl, M. J. C. van Gemert, and A. J. Welch, ''Determining the optical properties of turbid media by using the adding-doubling method,'' *Appl. Opt.* **32**, 559–568 (1993).
20. B. C. Wilson and S. L. Jacques, ''Optical reflectance and transmittance of tissues: principles and applications,'' *IEEE J. Quant. Elect.* **26**, 2186–2199 (1990).
21. C. F. Bohren and D. R. Huffman, *Absorption and Scattering of Light by Small Particles*, Wiley, New York (1983).
22. Polyscience Inc. *Particle Catalog*, p. 25 (1995–96).
23. A. M. K. Nilsson, R. Berg, and S. Andersson-Engels, ''Measurements of the optical properties of tissue in conjunction with photodynamic therapy,'' *Appl. Op.* **34**, 4609–4619 (1995).
24. J. H. Torres, A. J. Welch, I. Cilesiz, and M. Motamedi, ''Tissue optical property measurements: overestimation of absorption coefficient with spectrophotometric techniques,'' *Lasers Surg. Med.* **14**, 249–257 (1993).
25. V. G. Peters, D. R. Wyman, M. S. Patterson, and G. L. Frank, ''Optical properties of normal and diseased human breast tissues in the visible and near infrared,'' *Phys. Med. Biol.* **35**, 1317–1334 (1990).
26. L. W. Dalton, D. L. Page, and W. D. Dupont, ''Histologic grading of breast carcinoma: a reproducibility study,'' *Cancer* **73**, 2765–2770 (1994).
27. W. J. Lennington, R. A. Jensen, L. W. Dalton, and D. L. Page, ''Ductal carcinoma of the breast: heterogeneity of individual lesions,'' *Cancer* **73**, 118–124 (1994).
28. M. J. C. van Gemert, S. L. Jacques, H. J. C. M. Sterenborg, and W. M. Star, ''Skin optics,'' *IEEE Trans. Biomed. Eng.* **36**, 1146–1154 (1989).
29. A. H. Gandjabkhche, R. Nossal, R. Dadmarz, D. Schwartzentruber, and R. F. Bonner, ''Expected resolution and detectability of adenocarcinoma tumors within human breast in time-resolved images,'' *Proc. SPIE* **2387**, 111–118 (1995).
30. C. L. Burch, ''Monte Carlo simulations of photon migration in highly scattering media,'' Masters thesis, Vanderbilt University, Nashville, TN (1993).
31. M. Keijzer, W. M. Star, and P. R. M. Storchi, ''Optical diffusion in layered media,'' *Appl. Opt.* **27**, 1820–1824 (1988).
32. M. S. Patterson, S. J. Madsen, J. D. Moulton, and B. C. Wilson, ''Diffusion equation representation of photon migration in tissue,'' *IEEE MTT-S Int. Microwave Symp. Dig.* **2**, 905–908 (1991).
33. B. C. Wilson, E. M. Sevick, M. S. Patterson, and B. Chance, ''Time dependent optical spectroscopy and imaging for biomedical applications,'' *Proc. IEEE* **80**, 918–930 (1992).
34. J. Folkman, ''Angiogenesis and breast cancer,'' *J. Clin. Oncol.* **12**, 441–443 (1994).
35. D. L. Page and T. J. Anderson, *Diagnostic Histopathology of the Breast*, Churchill Livingstone, New York (1987).

Acknowledgment: The Publishers wish to acknowledge permission received from publishers and authors to reproduce figures used in this paper.